STRUCTURE AND PROPERTIES OF TiAl-BASED ALLOYS DOPED WITH 2 at.% Mo

M.V. Remez,[1,3] Yu.M. Podrezov,[1] A.A. Bondar,[1] V. Witusiewicz,[2] U. Hecht,[2] N.I. Tsyganenko,[1] O.O. Bilous,[1] and V.M. Petyukh[1]

UDC 669.295:620.171

Arc-melted $Ti_{100-x}Mo_2Al_x$ alloys (where x is 44, 46, 48, and 50 at.% Al) that were produced from pure components were examined by X-ray diffraction and scanning electron microscopy with electron microprobe analysis (SEM/EDX). The melting points and solid-phase transformations were studied by differential thermal analysis (DTA) and the mechanical properties by fracture toughness, bending, and compression tests. The CALPHAD approach was used for thermodynamic calculation of phase equilibria in the composition region under study. The cast alloys mainly consist of a lamellar structure formed by lamellas of γ-TiAl and $α_2$-Ti_3Al phases with submicron thickness and a cubic $Ti_{55}Mo_4$–$6Al_{39-40}$ phase of A2 type (β) or B2 type (β0). In the γ-TiAl-based alloys, molybdenum behaves as a low-melting dopant, enriching the grain periphery. The standard mechanical characteristics of the alloys were determined and their structural sensitivity was analyzed. All studied alloys demonstrate excellent high-temperature strength. The yield stress is 400–600 MPa in the temperature range 20–750°C. The strength slightly increases at 300 and 600°C under dynamic strain ageing. The strain hardening parameters were established over a wide range of test temperatures. The temperature dependence of the strain hardening coefficient and strain hardening index was analyzed for alloys in different phase and structural states. In the temperature range from 20 to 600°C, the strain hardening index and coefficient were found to vary slightly. The strain hardening index increased from n = 0.6 to n = 0.95 with aluminum content changing from 44 to 50 at.%, which indicates that the strain hardening mechanism changes with variation in the alloy phase constituents.

Keywords: *TiAl, intermetallics, Al–Mo–Ti, phase constituents, lamellar structure, high-temperature strength, ductility, fracture toughness, strain hardening.*

INTRODUCTION

Molybdenum-doped γ-TiAl-based materials are promising for high-temperature applications as they have low density and possess high-temperature strength and creep and oxidation resistance [1–5]. Even small molybdenum additions are known to favorably influence the high-temperature strength, heat resistance, and rupture resistance [4], ductility [5], and capability to deform under thermomechanical loads [6]. Additions of molybdenum

[1]Frantsevich Institute for Problems of Materials Science, National Academy of Sciences of Ukraine, Kyiv, Ukraine. [2]ACCESS e.V., Aachen, Germany.

[3]To whom correspondence should be addressed; e-mail: r7marine@gmail.com.

and other β-stabilizers need to be limited in order that these alloys could have the optimum phase constituents—such as lamellas of the γ- and $α_2$-phases—and brittle cubic β (A2) or $β_0$ (B2) phases would not deteriorate the properties. Calculations with the equation provided in [2] yield a maximum molybdenum content of 2 at.% and maximum niobium content of 8 at.%. The γ-TiAl-based alloys containing half the maximum content of molybdenum and niobium, 1 at.% Mo and 4 at.% Nb, and those containing 0.1 at.% B, being known as TNM, are considered to be most promising [6–10].

Despite the interest in alloys in the $γ + α_2$ and $γ + α_2 + β/β_0$ phase regions, there is a lack of published papers focusing on systematic studies of composition dependences for the structure and mechanical properties of Ti−Mo−Al alloys in the respective composition range.

The objective of this research effort is to examine the effect of aluminum content on the phase composition, structure, and mechanical properties of titanium aluminide alloys doped with 2 at.% Mo.

EXPERIMENTAL PROCEDURE

We examined TiAl-based alloys with the same molybdenum content (2 at.%) and different aluminum and titanium contents: $Ti_{98−x}Mo_2Al_x$, where x = 44, 46, 48, or 50 at.% (Table 1). Ingots 20 g in weight were produced by melting together iodide-refined titanium (99.9 wt.% Ti), lump aluminum (99.99 wt.% Al), and molybdenum rods (99.9 wt.% Mo). Molybdenum was introduced as the $Mo_{47.3}Al_{52.7}$ dopant that was melted in the same way as the alloys. The oxygen content of the alloys determined by reduction extraction in a nickel bath followed by chromatographic analysis ranged from 0.05 to 0.1 wt.%. In all cases, the nitrogen and hydrogen contents did not exceed the sensitivity limits: 0.001 wt.% N and 0.003 wt.% H. The carbon content found by alkali titration of the residue resulting from the adsorption of CO_2 formed in oxidation of the samples was 0.06–0.11 wt.%.

The samples were melted in an arc furnace with a nonconsumable tungsten electrode on a water-cooled copper hearth. To be homogeneous, the ingots were melted and tilted three times, ground, and melted again in the same way. The cooling rate was ~100 °C/sec. The melting weight loss was 0.05–0.22 wt.%. The alloy compositions defined by the loss and measured with a scanning electron microscope (SEM/EDX) showed that deviation of the aluminum content from the nominal value was no more than 0.2 at.% and the deviation of the molybdenum content no more than 0.1 at.%. Hence, the composition of the alloys was taken as that of the starting charge.

The constitution of the melted alloys was examined by X-ray diffraction (XRD) and metallography, including optical and scanning electron microscopy employing a ZEISS-LEO Gemini 1550 microscope (Karl Zeiss, Inc., Germany) equipped with an INCA Microanalysis System (Oxford Instruments). The chemical composition of the alloys and structural components was determined from energy-dispersive spectra (SEM/EDX). X-ray diffraction patterns for sections were taken with a DRON-3 diffractometer in filtered copper radiation. The phase composition of the alloys was defined with full-profile analysis of the X-ray diffraction patterns carried out with the PowderCell-2 software.

TABLE 1. Results of X-Ray Diffraction for Ti−Mo−Al Alloys

Alloy No.	Alloy composition, at.%			Phase constituents, wt.%	Lattice parameters, pkm				
					γ		$α_2$		$β/β_0$
	Ti	Mo	Al		a	c	a	c	a
1	54	2	44	35 γ + 58 $α_2$ + 7 β	397.8	402.9	572.6	462.1	319
2	52	2	46	77 γ + 19 $α_2$ + 4 β	401.4	405.4	576	462	323
3	50	2	48	73 γ + 25 $α_2$ + 2 β	400.9	406.6	575	462	322
4	48	2	50	86 γ + 13 $α_2$ + 1 β	399.1	406.7	573	456	317

The melting points and solid-phase transformation temperatures were studied by differential thermal analysis (DTA) employing the apparatus with a W/W–Re20% wire thermocouple described in [11, 12]. The experiments were performed in a high-purity helium atmosphere at a heating and cooling rate of 20 °C/min using Sc_2O_3 crucibles. Solid-phase transformation temperatures were also determined with a DSC 404 F3 Pegasus differential scanning calorimeter (NETZSCH, Germany) in the DTA mode. The experiment was performed in Y_2O_3 crucibles in an argon atmosphere of 6N purity at a rate of 20 K/min. The Pt–Rh sensor was calibrated at the same heating rate as that of In, Sn, Zn, Al, Ag, Au, and Ni pure metals.

Three-point-bending tests to determine fracture toughness and bending strength were performed at room temperature at a relative strain rate of $2 \cdot 10^{-3}$ sec^{-1} on standard 3 mm × 5 mm × 20 mm samples employing a Ceramtest machine (Special Design and Engineering Office of the Institute of Strength Problems, National Academy of Sciences of Ukraine). An atomically sharp crack was induced by electrospark cutting.

Compression tests were performed in the temperature range from 20 to 750°C at a relative strain rate of $0.5 \cdot 10^{-3}$ sec^{-1} on 2 mm × 2 mm × 4 mm rectangular samples using a U22-52 testing machine (Special Design and Engineering Office of the Institute of Strength Problems, National Academy of Sciences of Ukraine). The primary 'force–displacement' curves were used to plot the 'stress–strain' curves to determine standard mechanical compression properties.

EXPERIMENTAL RESULTS ON ALLOY CONSTITUTION

Figures 1 and 2 show microstructures of the alloys and their phase constituents determined with EDX. Table 1 indicates alloy phase constituents according to X-ray diffraction (XRD). In all alloys, α_2-Ti_3Al- and γ-TiAl-based phases and a cubic $Ti_{55}Mo_{4-6}Al_{39-40}$ phase were found. The small amount of the cubic phase does not allow its structural type to be identified using X-ray diffraction patterns: A2 structure of W (β) type or B2 structure of CsCl (β_0) type. With greater aluminum content of the alloys, the amount of the γ-phase predictably increases and that of the α_2 and β/β_0 phases decreases. The cubic phase content is at the level of XRD sensitivity (about 1 wt.%) in alloy 4 ($Ti_{48}Mo_2Al_{50}$) with the greatest aluminum amount. Attention should be focused on some difficulties in interpreting X-ray data: the most intensive reflections of the β/β_0 and α_2 phases with (110) and (002) indices are close to each other—$2\theta = 39.4$–$40.2°$ and 41.1–$41.4°$ (copper radiation)—and are located on the shoulder of the most intensive peak of the γ-phase with a vertex at $2\theta = 38.8$–$39.0°$. It should be noted that the X-ray diffraction patterns taken from alloy sections and the texture resulting from the orientation of lamellas relative to the crystallization front distort the phase ratios found.

Upon study of the alloy compositions (Figs. 1 and 2, Table 1), we can conclude that the cast alloys primarily consist of a lamellar structure formed by lamellas of α_2- and γ-phases of submicron thickness. The brighter cubic β/β_0-phase enriched with heavier molybdenum and depleted of lighter aluminum precipitated at intergrain and subgrain boundaries of high-temperature α- and β-phases, whose decomposition led to the lamellar structure.

A thermodynamic description was developed in [13] for the ternary Ti–Mo–Al system. It was used to perform thermodynamic calculations and present fragments of the isothermal section of the phase diagram at 1050°C (Fig. 3), a vertical section at the 2 at.% Mo isopleth (Fig. 4), and phase composition of each alloy studied in the temperature range 800−1600°C (Fig. 5). A comparison of Table 1 and Figs. 2, 3, and 5 indicates that the isothermal section at 1050°C adequately presents the phase composition of the cast alloys and phase constituents. Hence, the state of the cast alloys 'freezes' at this temperature when they are cooled down. This is consistent with our previous results for the γ-TiAl alloys doped with niobium and tantalum [16] and with niobium and chromium [17].

Differential thermal analysis revealed intensive thermal effects from melting of the alloys. These effects agree well with the solidus and liquidus lines plotted at the vertical section (Fig. 4). Effects of solid-phase transformations were recorded; the transformation of the α-phase into the β-phase in heating (and vice versa in cooling) and the formation (decomposition) of the α-phase were most intensive. The temperature of peritectic
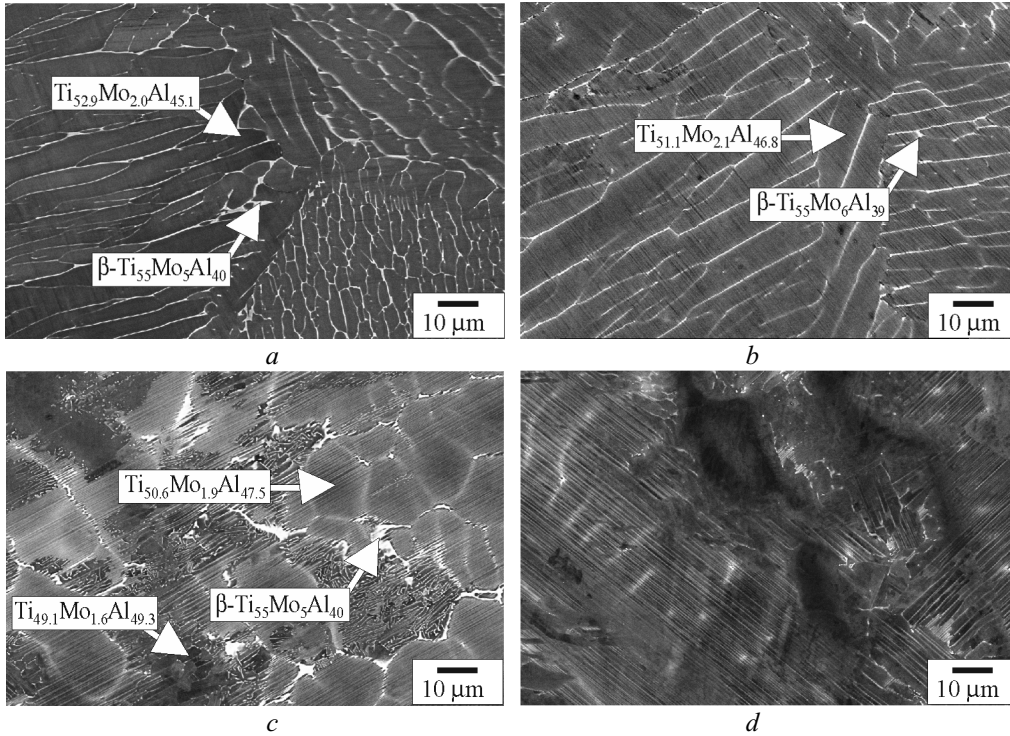
Fig. 1. Microstructure of alloys 1 (*a*), 2 (*b*), 3 (*c*), and 4 (*d*) in backscattered electrons and composition of structural components determined by electron microprobe analysis with SEM/EDX (the numbering of alloys here and in subsequent figures corresponds to Table 1)
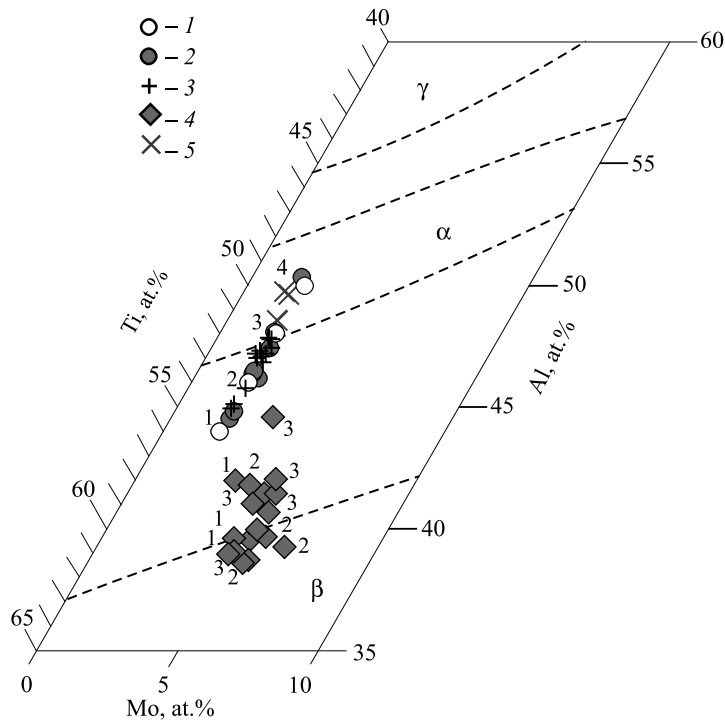

Fig. 2. Composition of alloys 1–4: *1*) nominal; *2*) according to SEM/EDX; and *3*) superfine structure resulting from eutectoid decomposition of the α-phase; *4*) β-phase; and *5*) γ-phase
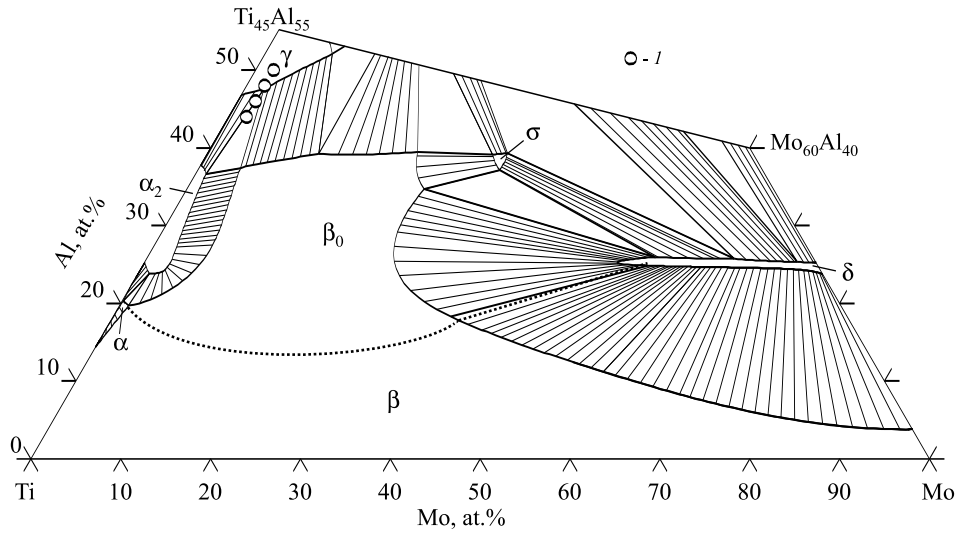
Fig. 3. Fragment of the isothermal section of the Ti−Mo−Al phase diagram at 1050°C calculated according to the thermodynamic description [13]: *1*—composition of the alloys studied

reaction L + β ↔ α at 2 at.% Mo is 1477°C (Fig. 4). This is 14°C lower than in the binary Ti−Al system [18]. In the γ-TiAl-based alloys, molybdenum behaves as a low-melting dopant similarly to chromium [17], enriching the grain periphery, which we can observe on the microstructures of the cast alloys.
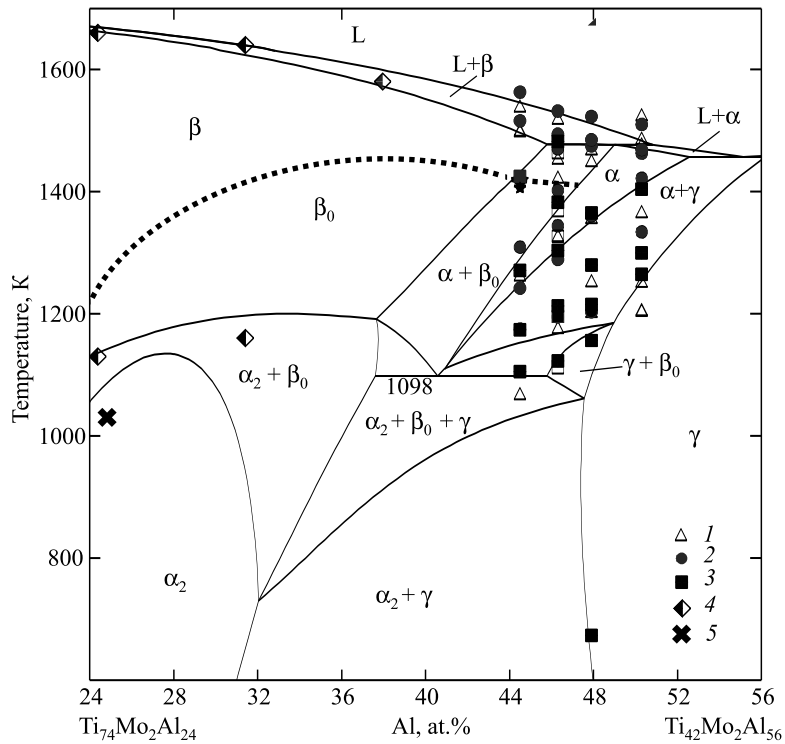

Fig. 4. Fragment of the isothermal section of the Ti−Mo−Al phase diagram along the 2 at.% Mo isopleth calculated according to the thermodynamic description [13]: *1)* DTA data for the cast alloys (this paper); *2)* DTA data for the alloys annealed at subsolidus temperatures [13]; *3)* DSC data for the same alloys annealed at subsolidus temperatures [13]; *4)* and *5)* DTA data from the papers [14] and [15], respectively

EXPERIMENTAL RESULTS ON ALLOY PROPERTIES

Mechanical Properties of the Alloys at Room Temperature Determined by Bending Tests. Table 2 provides the main mechanical characteristics of the $Ti_{98-x}Mo_2Al_x$ alloys tested by bending at room temperature: elastic modulus E, proportionality limit σ_{001}, yield stress σ_{02}, bending strength σ_{max}, plastic strain to fracture ε_{pl}, and fracture toughness K_{Ic}.

Figure 6 presents composition dependences for fracture toughness, ductility, and bending strength. All alloys are of extreme nature. The maximum fracture toughness and ductility are exhibited by the alloy with 48 at.% Al. This result agrees well with the literature [19, 20] and our data obtained previously for the Ti–Al–Nb–Cr alloys [17, 16]. According to [21], the greater fracture toughness at 48 at.% Al is attributed to features peculiar to the interaction between the lamellas and crack [4]. The crack is arrested as twins form in the ductile region. This crack propagation mechanism in the alloys with 48 at.% Al improves the strength and ductility at room temperature. These characteristics are maximum (determined at the moment of fracture) and are directly associated with the crack propagation features. Given the increased properties of the cast alloys with 48 at.% Al at room temperature, exactly this content was considered to be most promising for third-generation alloys [4] (for example, 48 Ti–48 Al–2 Nb–2 Cr alloy).

Note that the mechanical properties at room temperature are affected by the brittle β-phase, whose amount increases in alloys with low aluminum content (7 and 4 wt.% at 44 and 46 at.% Al, respectively) thus decreasing ductility compared to other alloys in the system.

Compression Tests of the Ti–Al–Mo System over a Wide Temperature Range. Bending tests do not allow the plastic strain mechanisms and structural sensitivity of strain hardening to be studied because materials in this class have extremely low strain to fracture. Compression tests are much more informative. Since the crack propagation process is complicated with this test pattern, fracture of the TiAl intermetallics is preceded by their significant plastic strain [21].

Compression tests of the alloys were performed in compliance with standard procedure in the temperature range 20–750°C. Table 3 summarizes the mechanical characteristics at room temperature. Even in the most brittle states, the compression test samples demonstrate noticeable plastic strain δ, which depends on the aluminum

TABLE 2. Mechanical Characteristics at Room Temperature for the Ti–Mo–Al Cast Alloys
Based on Bending and Fracture Toughness Tests

Alloy, at.%	E, GPa	σ_{001}, MPa	σ_{02}, MPa	σ_{max}, MPa	ε_y, %	K_{Ic}, MPa·m$^{0.5}$
$Ti_{54}Mo_2Al_{44}$	117	–	–	402	0	10.5
$Ti_{52}Mo_2Al_{46}$	139	559	–	591	0.017	17.2
$Ti_{50}Mo_2Al_{48}$	139	624	955	1005	0.288	23.7
$Ti_{48}Mo_2Al_{50}$	138	370	–	458	0.059	10.6

TABLE 3. Mechanical Characteristics at Room Temperature for the Ti–Mo–Al Cast Alloys
Based on Compression Tests

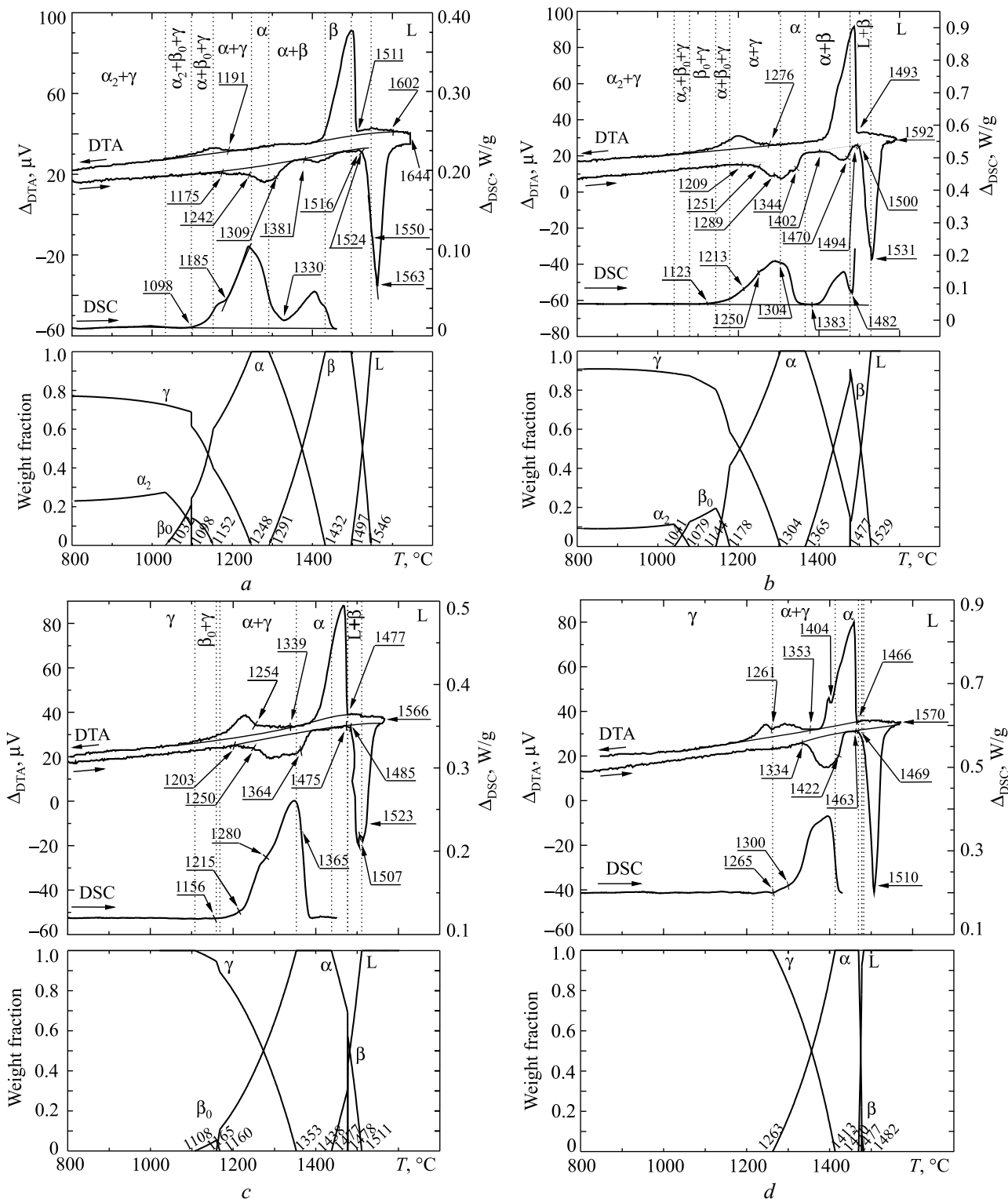| Alloy, at.%	σ_{max}, MPa	σ_{001}, MPa	σ_{02}, MPa	δ, %
$Ti_{54}Mo_2Al_{44}$	1564	566	693	6.8
$Ti_{52}Mo_2Al_{46}$	1354	409	578	8.4
$Ti_{50}Mo_2Al_{48}$	1829	489	577	24.6
$Ti_{48}Mo_2Al_{50}$	2258	389	459	29.3

Fig. 5. DTA and DSC curves and phase composition of Ti–Mo–Al alloys 1 (*a*), 2 (*b*), 3 (*c*), and 4 (*d*) calculated in the temperature range 800–1600°C according to the thermodynamic description [13]

content, monotonically increasing from 6.8% for the alloy with 44 at.% Al to 29.3% for the alloy with 50 at.% Al. On the contrary, yield stress σ_{02} monotonically decreases with greater aluminum content, while the compression strength monotonically increases.
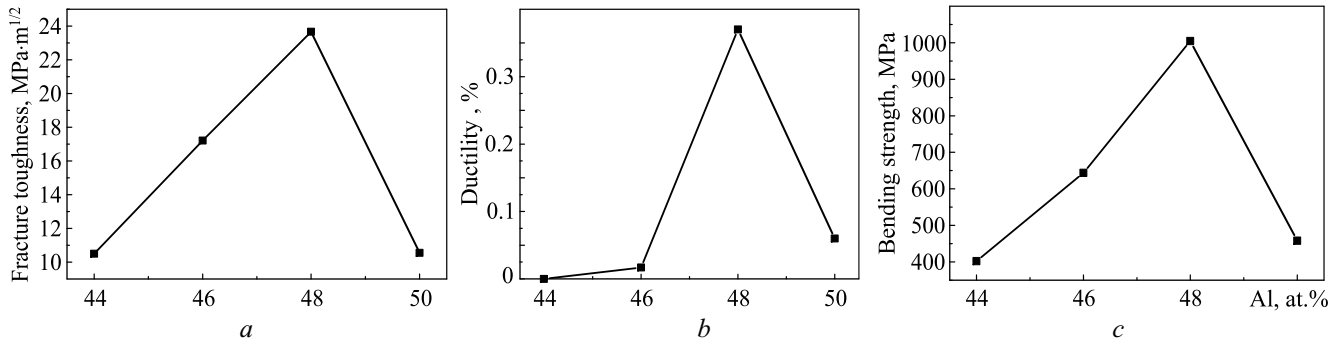
Fig. 6. Composition dependences of the mechanical characteristics of cast Ti–Mo–Al alloys based on bending tests at room temperature
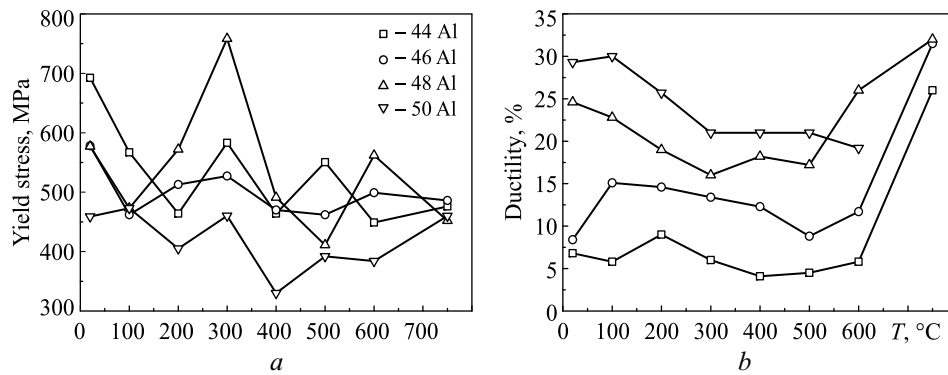

Fig. 7. Temperature dependences of the yield stress (*a*) and ductility (*b*) of cast Ti–Mo–Al alloys based on compression tests

High-temperature tests showed that all studied alloys had great high-temperature strength (Fig. 7). The yield stress (Fig. 7*a*) remained consistently high up to 750°C and then somewhat reduced (by 10–20% compared to that at room temperature) for all alloys. The increase in strength of the alloys at 300 and 600°C is attributed to the dynamic strain ageing effects and the action of Kear–Wilsdorf locks [22], as was already observed in [16] for the alloys doped with niobium and tantalum. The ductility depends on the aluminum content (Fig. 7*b*). The dynamic ageing process is accompanied by an insignificant decrease in ductility in the range 200–600°C, which is the case for the Ti–Nb–Cr–Al alloys [17]. The only exception is the $Ti_{50}Mo_2Al_{48}$ alloy, whose ductility at 600°C is 26%.

Unlike bending or tension tests, none of the mechanical characteristics determined in compression experiments demonstrates extreme dependence on aluminum content. In this case, the microcrack origination and development mechanisms are not crucial for the maximum properties acquired by the material since stresses relax on strain-related defects.

Figure 8 presents true strain hardening curves that were calculated considering changes in current sizes of the sample being deformed and showing plastic strain separated from the total strain. These dependences establish relationship between the deforming stresses and plastic strain. The results demonstrate a sharp increase in the hardening rate ($d\sigma/de$) with lower aluminum content. In particular, the hardening rate for the alloy with 44% Al is three times as high as that for the alloy with 48 at.% Al. This effect is reproduced well at both small ($\delta < 0.5\%$) and great ($\delta > 3\%$) strains and, importantly, over a wide temperature range.

The strain to fracture in compression tests, δ_{comp}, was determined by the rate at which the deforming stress reached the maximum true fracture stress, σ_f. The hardening rate depends on the constitution of studied alloys and is defined by the evolution of strain defects. The fracture stress is instead determined by the critical defect size, which is commensurable with the grain size and depends little on aluminum content. Hence, the strain to fracture in
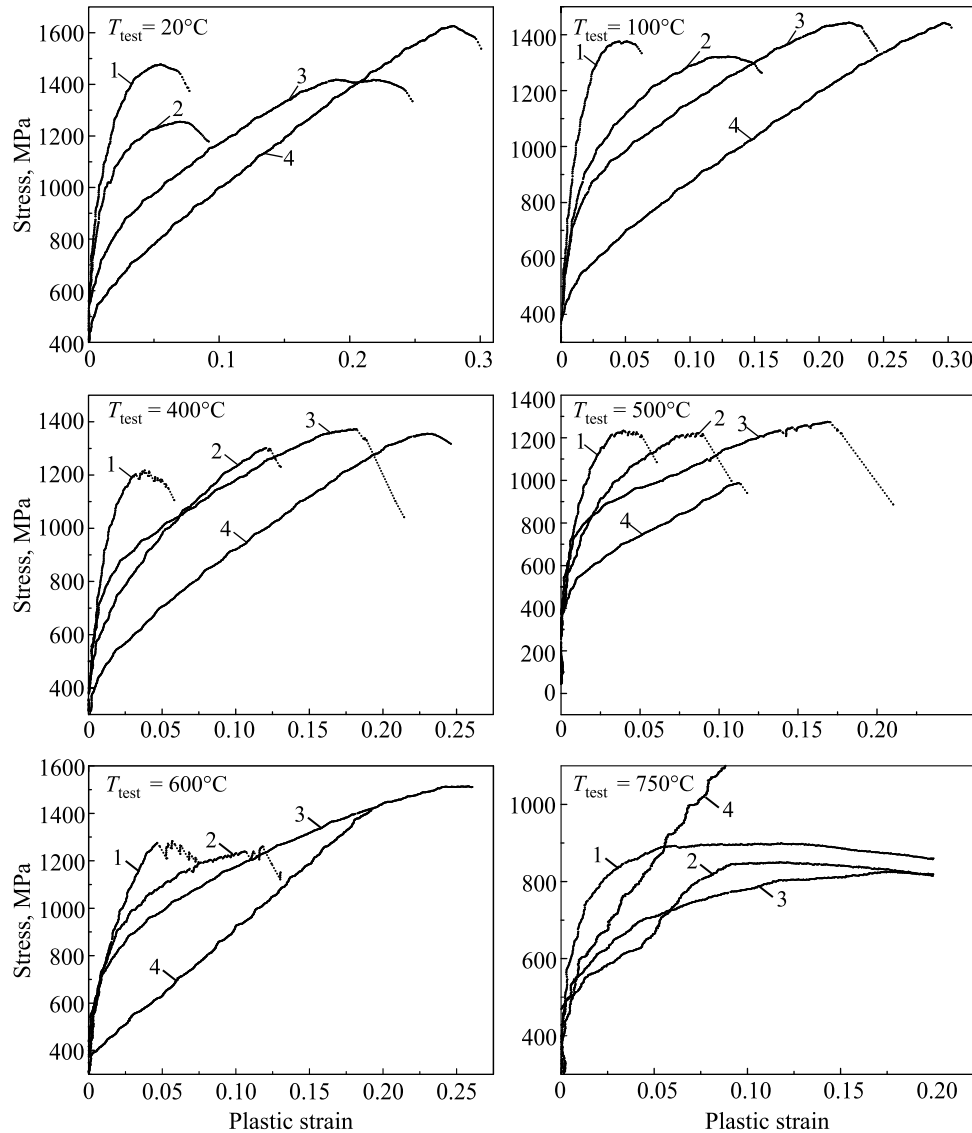
Fig. 8. Strain hardening curves for cast Ti–Mo–Al alloys 1–4 produced at different temperatures

compression should increase with aluminum content to the same extent as the hardening rate would decrease, as was observed experimentally.

The hardening features found at room temperature remain unchanged at elevated temperatures, in the range 20–500°C. The magnitude of stresses and strains does not change either. This indicates that the determining strain mechanisms remain unchanged in this temperature range.

The hardening curves for the alloys with 44–48 at.% Al demonstrate the same behavior at 600°C as at low temperatures, while the alloy with 50 at.% Al shows a much higher hardening rate. The hardening curves for the alloys with 44–48 at.% Al suggest that strain hardening degrades at 750°C when dislocation creep mechanisms change to diffusion-controlled ones. The alloy with 50 at.% Al demonstrates a further increase in hardening rate. These hardening features for the studied alloys are important since high-temperature tests were performed in the operating temperature range for aviation and space products.

Strain Hardening Index and Coefficient for γ-TiAl-Based Intermetallic Alloys. The data on the sensitivity of the hardening curves for the Ti–Al–Mo alloys to the aluminum content and the reproducibility of the established dependences for a wide temperature range indicate that the alloy composition has a substantial effect on strain hardening mechanisms. According to existing strain hardening theories, the shape of the loading curves is clearly

associated with the structural rearrangements in deformation. Trefilov–Moiseev's strain hardening theory [23–25] describes the strain hardening curves by parabolic law:

$$\sigma = \sigma_{02} + Ke^{n}, \tag{1}$$

where K is the strain hardening coefficient and n is the strain hardening index. In this equation, n is determined by the type of lattice. For bcc metals, $n = 0.5$ [23]; for fcc metals, n depends on the energy of stacking faults and varies widely for different materials: from 0.66 for aluminum to 0.95 for copper [25]. The situation is not so clear for hcp materials. In particular, n was found [26] to be equal to 0.92 for titanium of commercial purity regardless of the grain size in titanium alloys. However, doping of the alloy by elements that promote the formation of a small amount (up to 5%) of the bcc β-phase reduces the strain hardening index to 0.55. Kotko [26] indicates that the β-phase has the leading role in shaping the hardening curves and points out that the hardening index reduces most intensively when the β-phase is acicular or lamellar.

The hardening curves in Fig. 8 are parabolas described by Eq (1). Taking the logarithm of experimental data and presenting them in lnσ–lne coordinates allow parameter n to be determined by line slope and constant K by extrapolation to zero strain. The calculated results for the alloys deformed at 400°C are provided in Fig. 9. They indicate that the strain hardening index increases with higher aluminum content: $n = 0.6$ for the alloy with 44 at.% Al, $n = 0.76$ for the alloy with 46 at.% Al, $n = 0.83$ for the alloy with 48 at.% Al, and $n = 0.95$ for the alloy with 50% Al.

Therefore, the materials with low aluminum content demonstrate hardening indices typical of bcc metals and those with higher aluminum content show indices typical of fcc metals. Analysis of hardening mechanisms should take account of the following: when aluminum content increases from 44 to 50 at.%, the content of the γ-TiAl-based phase with an fcc-derived structure becomes 2.5 times higher. Doping elements in the TNB-type alloys are β-stabilizers, and the β-phase content decreases from ~7 to ~1 wt.% with higher aluminum content (Table 1). Results of electron microprobe analysis indicate that the alloy with low aluminum content has lamellar layers of the β-phase. The results agree with the findings provided in [26], where the decrease in strain hardening index n from 0.92 to 0.5 in doped titanium alloys is attributed to the presence of lamellar layers of the β-phase.
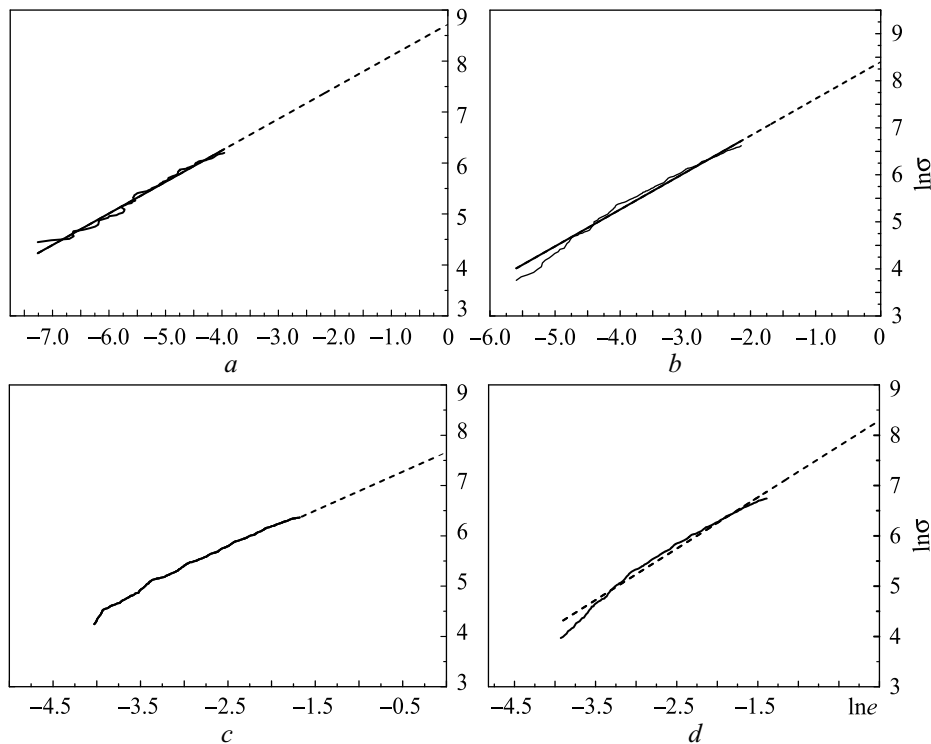

Fig. 9. Strain hardening curves for cast Ti–Mo–Al alloys 1 (*a*), 2 (*b*), 3 (*c*), and 4 (*d*) deformed at 400°C in logarithmic lnσ–lne coordinates
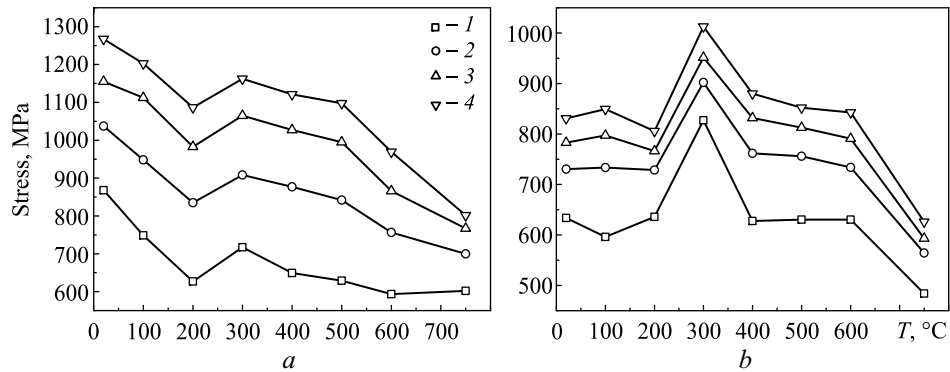
Fig. 10. Temperature sensitivity of the yield stress of $Ti_{54}Mo_2Al_{44}$ (*a*) and $Ti_{50}Mo_2Al_{48}$ (*b*) alloys corresponding to different compressive strains: 0.005 (*1*), 0.01 (*2*), 0.015 (*3*), 0.02 (*4*)

Temperature sensitivity of the yield stress at 0.5, 1, 1.5, and 2% strains was studied. Figure 10 shows these dependences for materials with 44 and 48 at.% Al. The yield stress was found to noticeably reduce with temperature in the alloy with 44 at.% Al, while temperature sensitivity of the yield stress is almost zero in alloys with greater aluminum content.

Linear fitting of the temperature sensitivity of yield stresses shows that the slope changes from 0.45 MPa/°C (for the alloys with low aluminum content) to almost zero (for the allows with high aluminum content). The line slopes at different plastic strains confirm the provisions of parabolic theory regarding the temperature sensitivity of the strain hardening coefficient.

The experimental deviation of some deforming stresses from the theoretical linear dependence is physically justified in most cases. In particular, stresses regularly increase at 300°C and rise at 500–600°C under Kear–Wilsdorf locks in γ-TiAl [18] and dynamic strain ageing effects [27].

The hardening features established for multicomponent γ-TiAl intermetallic-based alloys agree well with the existing ideas formulated for single-component bcc and fcc metals by Trefilov's scientific school [22]. This, in particular, applies to:

- potential fitting of the hardening curves to parabolic dependence (Eq. (1));
- sensitivity of strain hardening index *n* to the alloy phase composition and zero sensitivity to the testing temperature;
- sensitivity of strain hardening coefficient *K* to temperature for materials with low $n \approx 0.5$ (as for bcc metals) and linear fitting of this dependence at temperatures below the cold brittleness point (similarly to Trefilov–Milman's model of temperature sensitivity of the yield stress developed for bcc metals [24]).

CONCLUSIONS

The $Ti_{100-x}Mo_2Al_x$ alloys (where *x* is 44, 46, 48, and 50 at.% Al) mainly consist of a lamellar structure formed by lamellas of α_2- and γ-phases of submicron thickness and a cubic β/β_0-phase precipitated at intergrain and subgrain boundaries of high-temperature α- and β-phases. When aluminum amount changes from 44 to 50 at.%, the content of the α_2-phase decreases from 58 to 13 wt.%, that of the β-phase decreases from 7 to ~1 wt.%, and that of the γ-phase increases from 35 to 86 wt.%.

In mechanical tests at room temperature, the alloys show an extreme dependence of strength, ductility, and fracture toughness on aluminum content. The maximum mechanical characteristics are exhibited by the alloy with 48 at.% Al.

High-temperature tests have demonstrated that all alloys studied have great high-temperature strength. The yield stress is 400−600 MPa over the entire range of test temperatures. The strength somewhat increases at 300 and 600°C because of dynamic strain ageing and Kear–Wilsdorf locks.

The ductility depends on aluminum content and increases from 5% for the alloy with 44 at.% Al to 30% for the alloy with 50 at.% Al. The dynamic strain ageing process is accompanied by an insignificant decrease in ductility.

The hardening curves fit to a parabolic dependence. Strain hardening index n has been found to be sensitive to the alloy composition: n increases from 0.6 for the alloy with 44 at.% Al to 0.95 for the alloy with 50 at.% Al.

The strain hardening index is not sensitive to the test temperature, while strain hardening coefficient K of alloys with 44 and 46 at.% Al demonstrates temperature sensitivity but becomes no longer temperature-sensitive at greater aluminum content.

REFERENCES

1. S. Das, J.C. Mishurda, W.P. Allen, J.H. Perepezko, and L.S. Chumbley, "Development of a $(\gamma + \beta_0)$ lamellar microstructure in a $Ti_{45}Al_{50}Mo_5$ alloy," *Scr. Metall. Mater*., No. 28, 489–494 (1993).
2. F.-S. Sun, C.-X. Cao, M.-G. Yan, and S.-E. Kim, "Alloying mechanism of β stabilizers in a TiAl alloy," *Metall. Mater. Trans. A*, **32A**, 1573–1589 (2001).
3. I.S. Jung, H.S. Jang, M.H. Oh, J.H. Lee, and D.M. Wee, "Microstructure control of TiAl alloys containing β stabilizers by directional solidification," *Mater. Sci. Eng. A*, **329–331**, 13–18 (2002).
4. F. Appel, J.D.H. Paul, and M. Oehring, *Gamma Titanium Aluminide Alloys: Science and Technology*, Wiley–VCH Verlag GmbH&Co. KGaA, Weinheim (2011), p. 745.
5. R.K. Gupta, Bhanu Pant, and P. P. Sinha, "Theory and practice of $\gamma + \alpha_2$ Ti aluminide: A review," *Trans. Indian Inst. Met.*, **67**, No. 2, 143–165 (2014).
6. S. Mayer, P. Erdely, F. D. Fischer, D. Holec, M. Kastenhuber, T. Klein, and H. Clemens, "Intermetallic β-solidifying γ-TiAl based alloys—from fundamental research to application," *Adv. Mater.*, **19**, 1600735, 1–27 (2017).
7. H. Clemens, W. Wallgram, S. Kremmer, V. Güther, A. Otto, and A. Bartels, "Design of novel β-solidifying TiAl alloys with adjustable β/B2-phase fraction and excellent hot-workability," *Adv. Eng. Mater.*, **10**, No. 8, 707–713 (2008).
8. H. Clemens and S. Mayer, "Design, processing, microstructure, properties, and applications of advanced intermetallic TiAl alloys," *Adv. Eng. Mater.*, **15**, 191–215 (2013).
9. T. Klein, L. Usategui, B. Rashkova, M.L. Nó, J. San Juan, H. Clemens, and S. Mayer, "Mechanical behavior and related microstructural aspects of a nano-lamellar TiAl alloy at elevated temperatures," *Acta Mater.*, **128**, 440–450 (2017).
10. S. Mayer, M. Kastenhuber, and H. Clemens, "Advanced titanium aluminides—how to improve the creep resistance via compositional and microstructural optimization," *Mater. Sci. Forum*, **941**, 1484–1489 (2018).
11. Ju. A. Kocherzhinsky, "Differential thermocouple up to 2450°C and thermographic investigations of refractory silicide," in: *Proc. Third ICTA (Davos). Thermal Analysis (Vol. 1)*, Birkhäuser Verlag, Basel (1971), pp. 549–559.
12. Ju.A. Kocherzhinsky, E.A. Shishkin, and V.I. Vasilenko, "DTA apparatus with a thermocouple sensor to 2200°C," in: *Phase Diagrams of Metallic Systems* [in Russian], Nauka, Moscow (1971), pp. 245–249.
13. V.T. Witusiewicz, U. Hecht, O.M. Stryzhyboroda, N.I. Tsyganenko, V.M. Voblikov, V.M. Petyukh, and T.Ya. Velikanova, "Thermodynamic re-modelling of the ternary Al–Mo–Ti system based on novel experimental data," *J. Alloys Compd.*, **749**, 1071–1091 (2018).
14. S.M. Ge, I.I. Kornilov, and E.N. Pylyaeva, "Study of the Ti–Al–Mo phase diagram in the region of titanium-rich alloys," *Zh. Neorg. Khim.*, No. 8, 366–372 (1963).
15. I.I. Kornilov, T.T. Nartova, and N. I. Shirokov, "Structure and properties of molybdenum-containing Ti_3Al aluminide," *Metalloved. Termoobrab. Met.*, No. 8, 40–42 (1969).
16. A.A. Bondar, V.T. Witusiewicz, U. Hecht, M.V. Remez, V.M. Voblikov, N.I. Tsyganenko, Ya.I. Evich, Yu.M. Podrezov, and T.Ya. Velikanova, "Structure and properties of titanium–aluminum alloys doped with niobium and tantalum," *Powder Metall. Met. Ceram.*, **50**, No. 7–8, 397–415 (2011).

17. M.V. Remez, Yu.M. Podrezov, A.A. Bondar, V.T. Witusiewicz, U. Hecht, V.M. Voblikov, N.I. Tsyganenko, Ya.I. Evich, and T.Ya. Velikanova, "Structure and properties of TiAl-based alloys doped with niobium and chromium," *Powder Metall. Met. Ceram.*, **55**, No. 1–2, 91–108 (2016).

18. V.T. Witusiewicz, A. A. Bondar, U. Hecht, S. Rex, and T.Y. Velikanova, "The Al–B–Nb–Ti system: III. Thermodynamic re-evaluation of the constituent binary system Al–Ti," *J. Alloys Compd.*, **465**, 64–77 (2008).

19. Z. Jin and T.R. Bieler, "Mechanical twinning in duplex Ti–48Al–2Nb–2Cr at 1038 K," *Mater. Res. Soc. Symp. Proc.*, **288**, 775–780 (1992).

20. M. Charpentier, D. Daloz, E. Gautier, G. Lesoult, A. Hazotte, and M. Grange, "Study of microstructure and solute partitioning in a cast Ti–48 Al–2 Cr–2 Nb alloy by quenching during directional solidification technique," *Metall. Mater. Trans. A*, **34**, No. 10, 2139–2148 (2003).

21. F. Appel, H. Clemens, and F.D. Fischer, "Modeling concepts for intermetallic titanium aluminides," *Prog. Mater. Sci.*, **81**, 55–124 (2016).

22. B.A. Greenberg and M.A. Ivanov, "The reasons for the unusual behavior of intermetallics during prestraining experiments," *Metallofiz. Noveish. Tekhnol.*, **21**, No. 7, 55–61 (1999).

23. V.F. Moiseev, "Effective strain hardening index of metals," *Metallofiz. Noveish. Tekhnol.*, **23**, 387–399 (2001).

24. V.I. Trefilov (ed.), V.F. Moiseev, E.P. Pechkovskii, I.D. Gornaya, and A.D. Vasiliev, *Strain Hardening and Fracture of Polycrystalline Metals* [in Russian], Naukova Dumka, Kyiv (1989), p. 256.

25. V.F. Moiseev, I.D. Gornaya, E.P. Pechkovskii, and V.I. Trefilov, "Some regular patterns of strain hardening of polycrystalline molybdenum alloys," *Probl. Prochn.*, No. 5, 77–82 (1986).

26. A.V. Kotko, "Strain hardening of doped titanium alloys," in: *Current Issues of Physical Materials Science: Collected Scientific Papers* [in Russian], Inst. Probl. Materialoved. NAN Ukrainy, Kyiv (2013), Issue 22, pp. 94–102.

27. B.V. Petukhov, "Dynamic strain ageing of materials with Peierls plasticity mechanism," *Zh. Tekh. Fiz.*, **86**, No. 9, 65–71 (2016).